

Teaching Recurrent Neural Networks to Modify Chaotic Memories by Example

Jason Z. Kim

Department of Bioengineering, University of Pennsylvania, Philadelphia, PA, 19104

Zhixin Lu

Department of Bioengineering, University of Pennsylvania, Philadelphia, PA, 19104

Erfan Nozari

*Department of Electrical and Systems Engineering,
University of Pennsylvania, Philadelphia, PA, 19104*

George J. Pappas

*Department of Electrical and Systems Engineering,
University of Pennsylvania, Philadelphia, PA, 19104*

Danielle S. Bassett

*Departments of Bioengineering, Physics & Astronomy,
Electrical & Systems Engineering, Neurology, and Psychiatry,
University of Pennsylvania, Philadelphia, PA, 19104
Santa Fe Institute, Santa Fe, NM 87501 and
To whom correspondence should be addressed: dsb@seas.upenn.edu*

(Dated: May 3, 2020)

Abstract

The ability to store and manipulate information is a hallmark of computational systems. Whereas computers are carefully engineered to represent and perform mathematical operations on structured data, neurobiological systems perform analogous functions despite flexible organization and unstructured sensory input. Recent efforts have made progress in modeling the representation and recall of information in neural systems. However, precisely how neural systems learn to modify these representations remains far from understood. Here we demonstrate that a recurrent neural network (RNN) can learn to modify its representation of complex information using only examples, and we explain the associated learning mechanism with new theory. Specifically, we drive an RNN with examples of translated, linearly transformed, or pre-bifurcated time series from a chaotic Lorenz system, alongside an additional control signal that changes value for each example. By training the network to replicate the Lorenz inputs, it learns to autonomously evolve about a Lorenz-shaped manifold. Additionally, it learns to continuously interpolate and extrapolate the translation, transformation, and bifurcation of this representation far beyond the training data by changing the control signal. Finally, we provide a mechanism for how these computations are learned, and demonstrate that a single network can simultaneously learn multiple computations. Together, our results provide a simple but powerful mechanism by which an RNN can learn to manipulate internal representations of complex information, allowing for the principled study and precise design of RNNs.

1 I. INTRODUCTION

2 Computers analyze massive quantities of data with speed and precision [1, 2]. At both the
3 hardware and software levels, this performance depends on fixed and precisely engineered
4 protocols for representing and executing basic operations on binary data [2–4]. In contrast,
5 neurobiological systems are characterized by flexibility and adaptability. At the biophysical
6 level, neurons undergo dynamic changes in their composition and patterns of connectivity
7 [5–8]. At the cognitive level, they abstract spatiotemporally complex sensory information to
8 recognize objects, localize spatial position, and even control new virtual limbs through expe-
9 rience [9–11]. Hence, neural systems appear to work on fundamentally different computing
10 principles that are learned, rather than engineered.

11 To uncover these principles, artificial neural networks have been used to study the repre-
12 sentation and manipulation of information. While feed-forward networks can classify input
13 data [12], biological organisms contain recurrent connections that are necessary to sustain
14 short-term memory of internal representations [13], allowing for more complex functions
15 such as tracking time, distance, and emotional context [14–18]. Further, recurrent neural
16 systems actually manipulate internal representations to simulate the outcome of dynamic
17 processes such as kinematic motion and navigation [19–21], and to decide between different
18 actions [22]. How do recurrent neural systems learn to represent and manipulate complex
19 information?

20 One promising line of work involves representing static memories as patterns of neural
21 activity, or *attractors*, to which a network evolves over time [23]. These attractors can exist
22 in isolation (e.g. an image of a face) or as a continuum (e.g. smooth translations of a face)
23 using Hopfield or continuous attractor neural networks (CANNs), respectively [24, 25]. Other
24 studies use a differentiable neural computer (DNC) to read and write information to these
25 attractor neural networks to solve complex puzzles [26]. For understanding neurobiological
26 systems, these memory networks are limited by requiring specifically engineered patterns of
27 connectivity, and cannot manipulate time-varying memories necessary to plan and produce
28 speech and music [27–29]. Additionally, DNCs artificially segregate the computing and
29 storage components. Hence, we seek a single neural system that learns to both represent
30 and manipulate temporally complex information by perceiving and replicating examples.

31 In this work, we use the *reservoir computing framework* [30] to obtain such a system

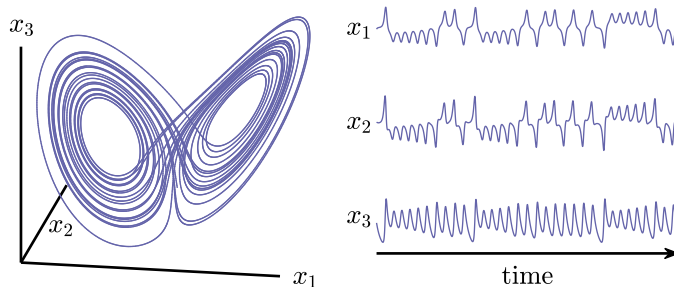
32 (the reservoir), where the complex information is a chaotic attractor that is not static,
 33 but evolves in a deterministic yet unpredictable manner through time [31]. Prior work
 34 has demonstrated the reservoir’s ability to represent and switch between isolated attractors
 35 by imitating examples [32, 33]. Here, we demonstrate that reservoirs can further learn to
 36 interpolate and extrapolate translations, linear transformations, and even bifurcations on
 37 their representations of chaotic attractor manifolds simply by imitating examples. Further,
 38 we put forth a mechanism of how these computations are learned, providing insights into the
 39 set of possible computations, and offering principles by which to design effective networks.

40 II. MATHEMATICAL FRAMEWORK

41 Neural systems represent and manipulate periodic stimuli through example, such as baby
 42 songbirds modifying their song to imitate adult songbirds [28]. However, they also perform
 43 more advanced and original manipulations on aperiodic stimuli with higher-order structure,
 44 such as musicians improvising on jazz melodies [29]. To model such complex stimuli, we use
 45 chaotic attractors that evolve deterministically yet unpredictably along a global structure:
 46 a fractional-dimensional manifold. Specifically, we consider the Lorenz attractor defined as

$$\begin{aligned}
 \dot{x}_1 &= \sigma(x_2 - x_1) \\
 \dot{x}_2 &= x_1(\rho - x_3) - x_2 \\
 \dot{x}_3 &= x_1x_2 - \beta x_3,
 \end{aligned}
 \tag{1}$$

47 and use the parameters $\sigma = 10, \beta = 8/3, \rho = 28$ from the original study [31] (Fig. 1).



48 FIG. 1. **Chaotic Lorenz manifold.** Lorenz attractor plotted in space (left) and time (right).
 49

50 Next, we model the neural system as a recurrent neural network driven by our inputs

$$\frac{1}{\gamma} \dot{\mathbf{r}} = -\mathbf{r} + \mathbf{g}(\mathbf{A}\mathbf{r} + \mathbf{B}\mathbf{x} + \mathbf{d}),$$

51 where \mathbf{r} is a real-valued vector of N reservoir neuron states, A is an $N \times N$ matrix of inter-
 52 neuron connections, B is an $N \times 3$ matrix of connections from the inputs to the neurons,
 53 \mathbf{d} is an $N \times 1$ bias vector, \mathbf{g} is a scalar activation function applied entry-wise to its input
 54 arguments (hence mapping vectors to vectors), and γ is a time constant.

55 Several prior studies use echo state [32] and FORCE learning [33] which allow reservoirs to
 56 predict a chaotic time series by modifying the inter-neuron connections. This modification
 57 can be accomplished by using the chaotic time series $\mathbf{x}(t)$ to drive the reservoir, thereby
 58 generating the reservoir time series $\mathbf{r}(t)$ (Fig. 2a,b). Here, $\mathbf{x}(t)$ and $\mathbf{r}(t)$ are $3 \times T$ and
 59 $N \times T$ matrices, respectively, from numerically evolving the differential equations over T
 60 time steps. By solving for a simple $3 \times N$ readout matrix W that uses linear combinations of
 61 reservoir states to approximate the input by minimizing the matrix 2-norm (see Supplement)

$$W = \underset{W}{\operatorname{argmin}} \|W\mathbf{r}(t) - \mathbf{x}(t)\|_2,$$

62 the output $\hat{\mathbf{x}}(t) = W\mathbf{r}(t)$ mimics the input $\mathbf{x}(t)$ (Fig. 2c). Finally, we close the feedback
 63 loop by substituting the output as the input to create the autonomous reservoir (Fig. 2d)

$$\frac{1}{\gamma}\dot{\mathbf{r}}' = -\mathbf{r}' + \mathbf{g}((A + BW)\mathbf{r}' + \mathbf{d}),$$

64 whose evolution projects to a Lorenz-shaped attractor as $\mathbf{x}'(t) = W\mathbf{r}'(t)$ (Fig. 2e). Hence,
 65 reservoirs sustain representations of complex temporal information by learning to au-
 66 tonomously evolve along a chaotic attractor from example inputs.

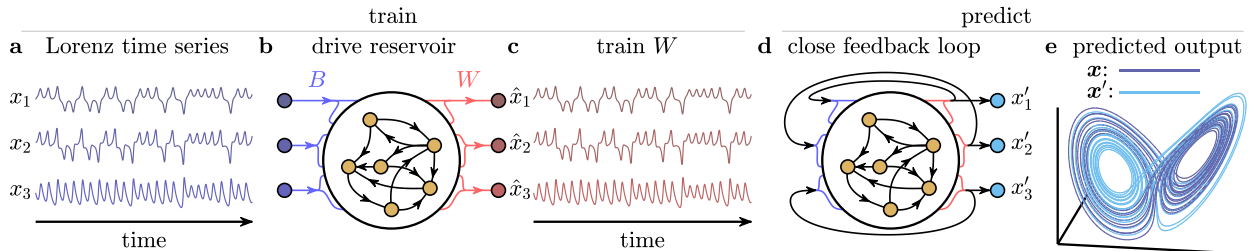


FIG. 2. **Representing chaotic attractors with reservoirs.** (a) Time series of a chaotic Lorenz attractor that (b) drives the recurrent neural network reservoir. (c) Weighted sums of the reservoir states are trained to reproduce the original time series. (d) By using these weighted sums of reservoir states to drive the reservoir instead of the inputs, (e) the reservoir autonomously evolves along a trajectory that projects to a Lorenz-shaped chaotic manifold.

67
68

69 To study how reservoirs might perform computations by modifying the position or ge-
 70 ometry of these representations in a desired way, we first adapt the framework to include a
 71 vector of control parameters \mathbf{c} that map to the reservoir neurons through matrix C to yield

$$\frac{1}{\gamma}\dot{\mathbf{r}} = -\mathbf{r} + \mathbf{g}(A\mathbf{r} + B\mathbf{x} + C\mathbf{c} + \mathbf{d}).$$

72 Such control parameters were also previously used to switch between multiple attractor
 73 outputs [33]. The second adaptation is to approximate the reservoir dynamics using a
 74 Taylor series to quadratic order around equilibrium values \mathbf{r}^* , $\mathbf{x}^* = \mathbf{0}$, $\mathbf{c}^* = \mathbf{0}$, yielding

$$\frac{1}{\gamma}\delta\dot{\mathbf{r}} = -\delta\mathbf{r} + U(A\delta\mathbf{r} + B\mathbf{x} + C\mathbf{c}) + V(A\delta\mathbf{r} + B\mathbf{x} + C\mathbf{c})^2. \quad (2)$$

75 Here, $\delta\mathbf{r} = \mathbf{r} - \mathbf{r}^*$, U , and V are diagonal matrices whose i -th entries are the first and half
 76 of the second derivatives of g_i evaluated at the fixed point, respectively, and $()^2$ is the entry-
 77 wise square of the vector (see Supplement for details). By studying quadratic reservoirs
 78 and how they learn to manipulate their representations of chaotic manifolds, we will gain
 79 an intuition due to their analytic tractability, and generalizability across many activation
 80 functions \mathbf{g} when driven within a range over which the quadratic expansion is accurate.

81 III. LEARNING A TRANSLATION OPERATION BY EXAMPLE

82 Reservoirs learn complex information through simple imitation: approximating the driv-
 83 ing inputs using the reservoir states is enough to autonomously represent and evolve about a
 84 chaotic manifold. Here we show that this simple scheme is also enough to learn to translate
 85 the representation. We begin with a Lorenz time series $\mathbf{x}_0(t)$, and create shifted copies

$$\mathbf{x}_c(t) = \mathbf{x}_0(t) + P\mathbf{c}. \quad (3)$$

86 For the purposes of demonstration, we consider a translation in the x_1 direction such that
 87 $P = [1; 0; 0]$ is a column vector, and $\mathbf{c} = 0, 1, 2, 3$ is a scalar. We use these four time series
 88 to drive our reservoir according to Eq. 2, thereby generating four reservoir time series $\mathbf{r}_c(t)$.
 89 Numerically, $\mathbf{x}_c(t)$ and $\mathbf{r}_c(t)$ are matrices of dimension $3 \times T$ and $N \times T$ over T time steps,
 90 which we concatenate along the time dimension into $\mathbf{x}(t) = [\mathbf{x}_0(t), \mathbf{x}_1(t), \mathbf{x}_2(t), \mathbf{x}_3(t)]$ and
 91 $\mathbf{r}(t) = [\mathbf{r}_0(t), \mathbf{r}_1(t), \mathbf{r}_2(t), \mathbf{r}_3(t)]$, respectively. Then, we compute output weights

$$W = \underset{W}{\operatorname{argmin}} \|W\mathbf{r}(t) - \mathbf{x}(t)\|_2, \quad (4)$$

92 such that our output $\hat{\mathbf{x}} = W\mathbf{r}(t)$ approximates our input $\mathbf{x}(t)$ (Fig. 3a–c). Finally, we
 93 substitute the output as the input to yield the feedback system (Fig. 3d)

$$\frac{1}{\gamma}\delta\dot{\mathbf{r}}' = -\delta\mathbf{r}' + U(R\delta\mathbf{r}' + C\mathbf{c}) + V(R\delta\mathbf{r}' + C\mathbf{c})^2, \quad (5)$$

94 where $R = A + BW$ (see Supplement for a discussion on $W\mathbf{r}_c(t) \approx W\delta\mathbf{r}_c(t)$).

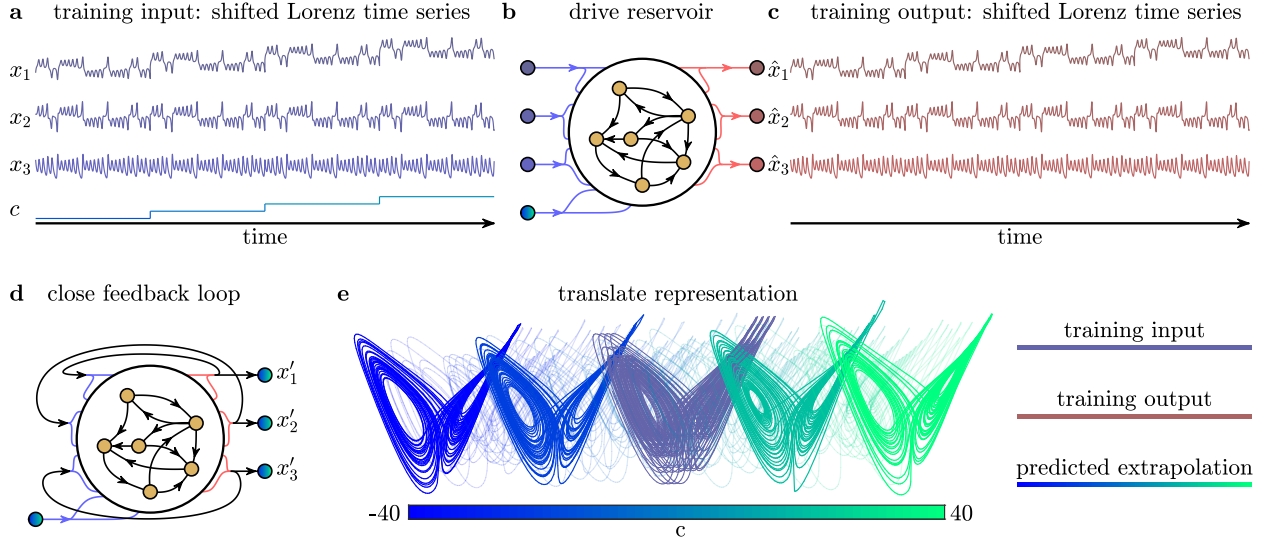


FIG. 3. **Learning and extrapolating a translation operation through examples.** (a) Schematic of the time series of the Lorenz and control inputs, beginning with the original Lorenz time series $\mathbf{x}_0(t)$ at $c = 0$, followed by three equally spaced shifts in the x_1 direction and in the c parameter. (b) These inputs generate four reservoir time series $\mathbf{r}_c(t)$. (c) Next, weighted sums of the reservoir states are used to generate outputs $W\mathbf{r}_c(t) = \hat{\mathbf{x}}_c(t) \approx \mathbf{x}_c(t)$ that mimic the inputs. (d) The outputs $W\mathbf{r}(t)$ replace the inputs $\mathbf{x}(t)$ to create a reservoir with a closed feedback loop. (e) Over the course of a single simulation, the reservoir evolves autonomously about a Lorenz-shaped manifold, and translates this representation along x_1 by smoothly and continuously changing c as a real number over a range much larger than the training range.

95 As we evolve this autonomous reservoir while varying c to extreme values $-40 \leq c \leq 40$
 96 both inside and outside of the training values, it has learned to evolve about a Lorenz-shaped
 97 manifold that is translated based on the value of c (see Supplement for translations in all
 98 spatial directions). Hence, by training the network on shifted copies of the input time series,
 99 the reservoir has learned a translation operation on the attractor.

100 **IV. LEARNING A LINEAR TRANSFORMATION OPERATION BY EXAMPLE**

101 In addition to learning a translation operation that does not change the geometry of the
 102 representation, here we demonstrate that reservoirs can learn linear transformation using
 103 the exact same framework. Similarly, we begin with a Lorenz time series $\mathbf{x}_0(t)$ generated
 104 from Eq. 1, and create linearly transformed copies of the time series such that

$$\mathbf{x}_c(t) = (I + cP)\mathbf{x}_0(t), \quad (6)$$

105 for $c = 0, 1, 2, 3$, where P is a matrix encoding a transformation (Fig. 4a,c). Specifically, we
 106 perform a squeeze along x_1 by setting $[P]_{11} = -0.012$ and the remaining elements to 0.

107 Exactly as before, we drive the reservoir according to Eq. 2, concatenate our input and
 108 reservoir time series into $\mathbf{x}(t)$ and $\mathbf{r}(t)$ to train the output weights W according to Eq. 4,
 109 and feed the outputs back as inputs to yield the feedback system Eq. 5. This reservoir
 110 autonomously evolves about a Lorenz-shaped manifold that stretches based on the parameter
 111 $-40 \leq c \leq 40$ (Fig. 4b,d) far outside of the parameters used in the training regime $c =$
 112 $0, 1, 2, 3$ (see Supplement for more examples). Hence, using the same framework, the reservoir
 113 has learned the linear transformation operation on the attractor manifold.

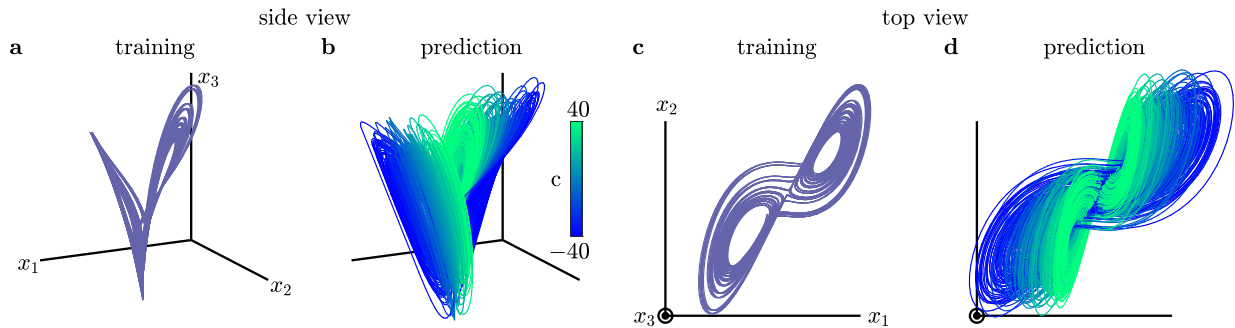
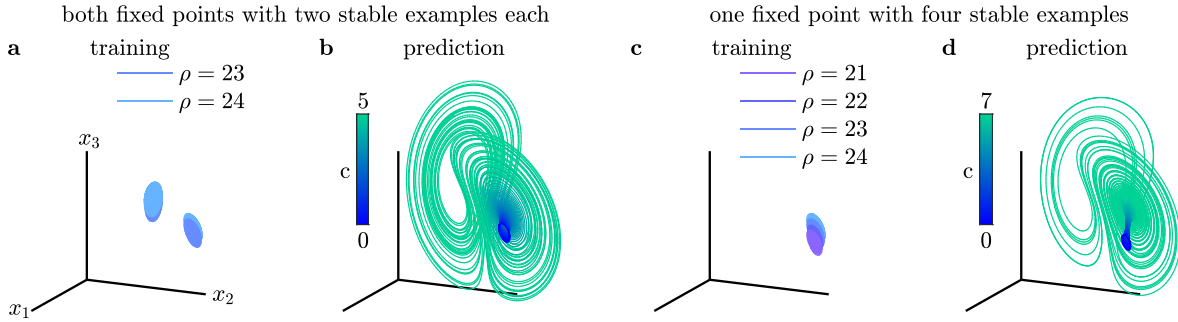


FIG. 4. **Extrapolating a transformation operation through examples.** (a) 3-dimensional plot of the training data of the Lorenz time series that has been stretched along the x_1 direction at $c = 0, 1, 2, 3$. (b) 3-dimensional plot of the feedback reservoir output that autonomously evolves about a Lorenz-shaped manifold that stretches dramatically based on varying c from -40 to 40 . We also provide a top view of the (c) training data and (d) predicted output data.

114 **V. LEARNING TO INFER A BIFURCATION BY EXAMPLE**

115 For both translations and transformations, the reservoir learned a smooth change in its
 116 representation of the chaotic manifold. Here we demonstrate that a reservoir can infer,
 117 without actually ever having experienced, a much more dramatic change: a bifurcation. In
 118 the Lorenz attractor (Eq. 1 for $\rho > 1, \sigma = 10, \beta = 8/3$), there are two fixed points: one at
 119 the center of each wing, which undergo a subcritical Hopf bifurcation when $\rho = \rho^* \approx 24.7$
 120 [23]. When $\rho < \rho^*$, these two fixed points are stable. When $\rho > \rho^*$, the fixed points become
 121 unstable, yielding the characteristic wing-shaped flow. Here we demonstrate that a reservoir
 122 trained only on stable examples ($\rho < \rho^*$) can accurately predict the unstable flow ($\rho > \rho^*$).



123 **FIG. 5. Extrapolating the bifurcation of the Lorenz.** (a) Two training trajectories for each
 124 of the stable Lorenz fixed points at the wings, for $\rho = 23$ with $c = 0$ (blue) and for $\rho = 24$ with
 125 $c = 1$ (light blue). (b) The predicted trajectory of the feedback reservoir moves towards a stable
 126 fixed point for $c = 0$, and bifurcates into a Lorenz-shaped manifold as c is increased. (c) Four
 127 training examples for one of the stable Lorenz fixed points for $\rho = 21, 22, 23, 24$ with $c = 0, 1, 2, 3$.
 128 (d) The predicted trajectory moves towards a stable fixed point for $c = 0$, and then bifurcates into
 129 a Lorenz-shaped manifold as c is increased.

125 For the two fixed points **a** and **b**, we begin with four training trajectories: $\mathbf{x}_{23}^a(t)$ and
 126 $\mathbf{x}_{23}^b(t)$ that evolve stably towards the fixed points for $\rho = 23$, and $\mathbf{x}_{24}^a(t)$ and $\mathbf{x}_{24}^b(t)$ that
 127 evolve stably towards the fixed points for $\rho = 24$ (Fig. 5a). We then drive the reservoir with
 128 $\mathbf{x}_{23}^a(t)$ and $\mathbf{x}_{23}^b(t)$ while setting $c = 0$, and with $\mathbf{x}_{24}^a(t)$ and $\mathbf{x}_{24}^b(t)$ while setting $c = 1$, and
 129 train the output weights. Finally, we evolve the feedback reservoir while changing c from 0
 130 to 5, and note that the trajectory bifurcates into a Lorenz-shaped manifold (Fig. 5b).

131 As a second demonstration, we begin with another set of four training trajectories:
 132 $\mathbf{x}_{21}^a(t), \dots, \mathbf{x}_{24}^a(t)$ that evolve stably towards only one fixed point for $\rho = 21, \dots, 24$ (Fig. 5c).

133 We then drive the reservoir with $\mathbf{x}_{21}^a(t), \dots, \mathbf{x}_{24}^a(t)$ while setting $c = 0, \dots, 3$, and train the
 134 output weights. Finally, we evolve the feedback reservoir while changing c from 0 to 7, and
 135 note that the trajectory again bifurcates into a Lorenz-shaped manifold (Fig. 5d). Hence,
 136 after only observing a few stable trajectories before the bifurcation ($\rho < \rho^*$), the reservoir
 137 accurately extrapolates the geometry of the Lorenz trajectory after the bifurcation ($\rho > \rho^*$).

138 VI. MECHANISM OF HOW OPERATIONS ARE LEARNED

139 Now that we have taught reservoirs to manipulate chaotic manifolds, we seek to under-
 140 stand the mechanism. We begin with some intuition by expanding the feedback dynamics

$$\frac{1}{\gamma} \delta \dot{\mathbf{r}}' = ([U + \underbrace{2V \text{diag}(C\mathbf{c})}_{\text{stretch}}]R - I)\delta \mathbf{r}' + \underbrace{UC\mathbf{c}}_{\text{shift}} + \underbrace{V(R\delta \mathbf{r}')^2 + V(C\mathbf{c})^2}_{\text{small}}$$

141 and notice that the control parameter can scale the shape of the reservoir's internal dynamics
 142 (stretch), and add a constant driving input (shift). For small changes in \mathbf{c} , the quadratic
 143 term $C\mathbf{c}$ is negligible. To formalize this intuition, we consider the time series $\mathbf{r}'(t) = \mathbf{r}'_{c=0}(t)$
 144 generated by evolving the autonomous reservoir according to Eq. 5 at $\mathbf{c} = \mathbf{0}$. Next, we take
 145 the total differential of Eq. 5 evaluated at $\mathbf{r}'(t)$ and $\mathbf{c} = \mathbf{0}$ to yield

$$(I - KA)d\mathbf{r}' + \frac{1}{\gamma} d\dot{\mathbf{r}}' = K(BWd\mathbf{r}' + Cdc), \quad (7)$$

146 where $K = U + 2V \text{diag}(R\delta \mathbf{r}'(t))$. Our goal is to write the change in the reservoir state
 147 $d\mathbf{r}'(t)$ that is induced by changing the control parameter by an infinitesimal amount dc .

148 When learning translations, the output weights are trained such that $W\mathbf{r}_c(t) \approx \mathbf{x}_c(t) =$
 149 $\mathbf{x}(t) + P\mathbf{c}$. For sufficiently nearby training examples (small P, \mathbf{c}), we also implicitly ap-
 150 proximate the differential relation $Wd\mathbf{r}(t) \approx Pdc$. Additionally, if the feedback reservoir
 151 stabilizes these examples, then $Wd\mathbf{r}'(t) \approx Pdc$. Substituting this relation into Eq. 7 yields

$$(I - KA)d\mathbf{r}' + \frac{1}{\gamma} d\dot{\mathbf{r}}' \approx K(BP + C)dc.$$

152 If we fix dc , we have $2N$ variables, $d\mathbf{r}'$ and $d\dot{\mathbf{r}}'$, but only N equations. By taking the time
 153 derivative of the differential relation, we generate another N variables and N equations.

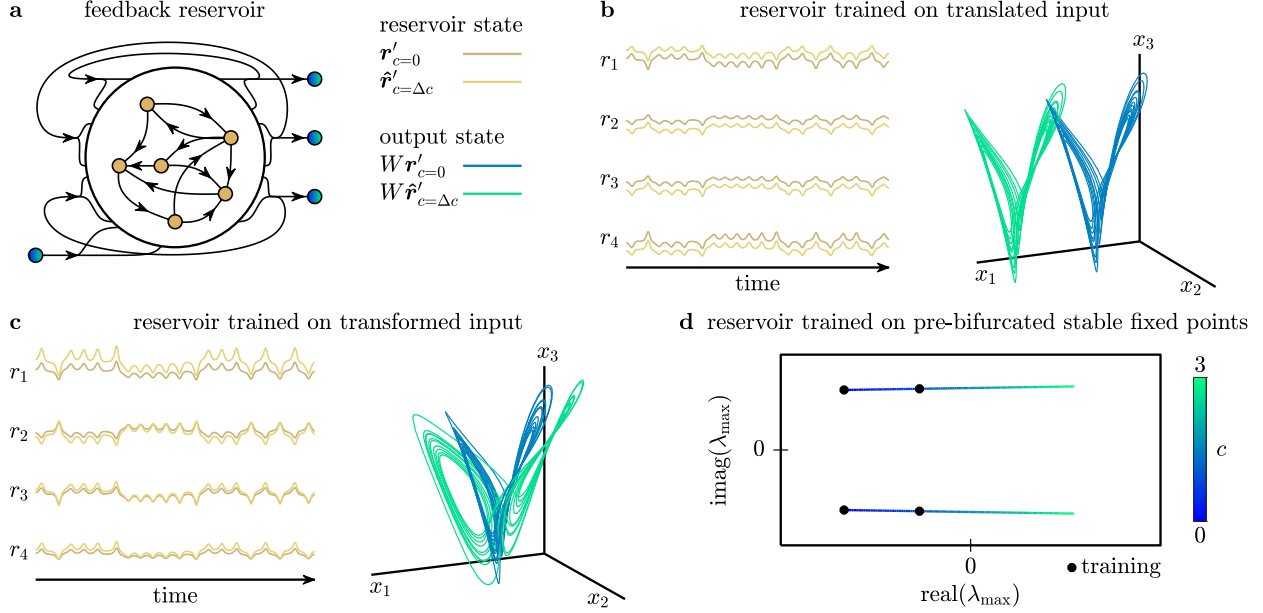


FIG. 6. **Changing the control parameter changes the reservoir dynamics to manipulate representations.** (a) Schematic of a reservoir with feedback connections after the output weights W have been trained. (b) Reservoir time series generated by evolving the autonomous reservoir with the original Lorenz input with $c = 0$ (dark gold). We also show the predicted time series from solving Eq. 8 after training on translated examples and setting $dc = \Delta c = 20$ (light gold). The output projections of the two time series are shown in blue and green, respectively. (c) The original and predicted reservoir states and their output projections for $\Delta c = -40$ after training on transformed Lorenz inputs by solving Eq. 9. (d) Plot of the real and imaginary components of the two most unstable eigenvalues of the autonomous reservoir trained on two stable Lorenz trajectories (Fig. 5a,b). The reservoir is linearized about its fixed point according to Eq. 10 as c is slowly changed.

154 Continuing to take time derivatives yields the following system of equations

$$\begin{bmatrix} H_0 & H_{-1} & 0 & \cdots \\ H_1 & H_0 & H_{-1} & \cdots \\ H_2 & 2H_1 & H_0 & \cdots \\ \vdots & \vdots & \vdots & \ddots \end{bmatrix} \begin{bmatrix} d\mathbf{r}' \\ d\dot{\mathbf{r}}' \\ d\ddot{\mathbf{r}}' \\ \vdots \end{bmatrix} \approx \begin{bmatrix} K \\ \dot{K} \\ \ddot{K} \\ \vdots \end{bmatrix} (BP + C)d\mathbf{c},$$

155 where $H_{-1} = \frac{1}{\gamma}I$, $H_0 = I - KA$, and $H_i = -K^{(i)}A$ is the i -th time-derivative of KA . This
 156 matrix is a block-Hessenberg matrix, with an analytic solution [34] for the first term $d\mathbf{r}'$.

157 We truncate this solution (see Supplement) to explicitly relate $d\mathbf{c}$ to $d\mathbf{r}'$ as follows:

$$d\mathbf{r}' \approx - \left[\gamma H_0^2 - H_1 \right]^{-1} \begin{bmatrix} -\gamma H_0 & I \end{bmatrix} \begin{bmatrix} K \\ \dot{K} \end{bmatrix} (BP + C)d\mathbf{c}. \quad (8)$$

158 As a demonstration, we pick a finite $\Delta\mathbf{c} = 20$, and plot the original and predicted change
 159 in the reservoir states, and their outputs in spatial coordinates (Fig. 6b). Hence, using only
 160 the feedback dynamics Eq. 5 and sufficiently nearby training examples, changing \mathbf{c} causes
 161 changes in the reservoir states from Eq. 8 that map to a translation.

162 The same approach can be used for linear transformations, where the output weights are
 163 trained such that $W\mathbf{r}_c(t) \approx \mathbf{x}_c(t) = (I + cP)\mathbf{x}(t)$. For sufficiently nearby training examples,
 164 we implicitly approximate the differential relation $Wd\mathbf{r}(t) \approx P\mathbf{x}(t)dc \approx PW\mathbf{r}(t)dc$, which
 165 if properly stabilized, yields $Wd\mathbf{r}'(t) \approx PW\mathbf{r}'(t)$. Performing the same time derivatives and
 166 solution truncation as in the translation, we get the following relation between dc and $d\mathbf{r}'$:

$$d\mathbf{r}' \approx - \left[\gamma H_0^2 - H_1 \right]^{-1} \begin{bmatrix} -\gamma H_0 & I \end{bmatrix} \begin{bmatrix} K(BPW\mathbf{r}' + C) \\ \dot{K}(BPW\mathbf{r}' + C) + KBPW\dot{\mathbf{r}}' \end{bmatrix} dc. \quad (9)$$

167 As another demonstration, we set $\Delta c = -40$, and plot the original and predicted change in
 168 the reservoir states, and their outputs (Fig. 6c).

169 Finally, to understand how the reservoir is able to infer a bifurcation, we demonstrate
 170 that it learns a smooth translation of eigenvalues. Specifically, at ρ^* , the fixed points at
 171 the wings of the Lorenz system undergo a Hopf bifurcation, whereby the real component of
 172 complex conjugate eigenvalues goes from negative to positive. To track the eigenvalues of
 173 the autonomous reservoir, we linearize Eq. 5 about a fixed point $\delta\mathbf{r}^*$ such that

$$\frac{1}{\gamma}\delta\dot{\mathbf{r}}' \approx [-I + UR + 2V\text{diag}(R\delta\mathbf{r}^* + C\mathbf{c})R](\delta\mathbf{r}' - \delta\mathbf{r}^*). \quad (10)$$

174 Then, using the output weights trained only on stable Lorenz trajectories (at $c = 0, \rho = 23$
 175 and $c = 1, \rho = 24$; Fig. 5a,b), we track the autonomous reservoir's two most unstable
 176 eigenvalues (largest real component) at the fixed point as we vary the control parameter
 177 from $c = 0$ to $c = 3$. We find that these eigenvalues are complex conjugates whose real
 178 components go from negative to positive (Fig. 6d). Hence, we demonstrate that not only
 179 can reservoirs learn smooth translations and transformations by mapping $d\mathbf{c}$ to $d\mathbf{r}'$, but they
 180 can also perform bifurcations by learning smooth changes in their eigenvalues.

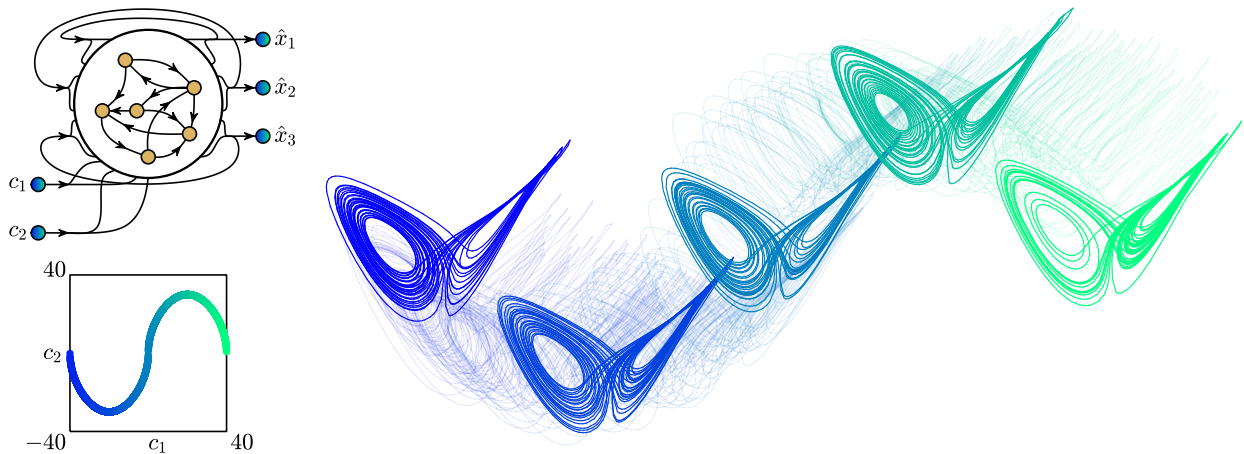


FIG. 7. **Flight of the Lorenz.** A reservoir trained on translated inputs along the x_1 and x_3 directions evolves autonomously along a Lorenz-shaped chaotic manifold. We can change the x_1 and x_3 position of its representation by changing control parameters c_1 and c_2 , respectively.

182 To close, here we demonstrate that reservoirs can easily learn multiple computations by
 183 changing multiple control inputs. We train a translation in the x_1 direction with control
 184 parameter c_1 , and a translation in the x_3 direction with control parameter c_2 . As before, we
 185 begin with a Lorenz time series $\mathbf{x}_{0,0}(t)$ generated from Eq. 1, and created shifted copies

$$\mathbf{x}_{c_1,c_2}(t) = \mathbf{x}_{0,0}(t) + c_1\mathbf{a}_1 + c_2\mathbf{a}_2,$$

186 where $\mathbf{a}_1 = [1; 0; 0]$ corresponds to an x_1 shift, and $\mathbf{a}_2 = [0; 0; 1]$ corresponds to an x_3 shift.
 187 We generate 10 shifted inputs, with one unshifted attractor ($c_1 = 0, c_2 = 0$), three shifts in
 188 the x_1 direction ($c_1 = 1, 2, 3, c_2 = 0$), three shifts in the x_3 direction ($c_1 = 0, c_2 = 1, 2, 3$),
 189 and three shifts in both directions ($c_1 = 1, 2, 3, c_2 = 1, 2, 3$). We use these shifted copies
 190 along with their corresponding control inputs to drive our reservoir and produce 10 reservoir
 191 time series $\mathbf{r}_{c_1,c_2}(t)$. Then, we concatenate these 10 time series into $\mathbf{x}(t)$ and $\mathbf{r}(t)$ to train
 192 output weights W according to Eq. 4, and perform the feedback according to Eq. 5 where
 193 $\mathbf{c} = [c_1; c_2]$ is a vector. By changing parameters c_1 and c_2 , the reservoir evolves about a
 194 Lorenz-shaped manifold that is shifted in the x_1 and x_3 directions (Fig. 7).

VIII. DISCUSSION

In this paper, we teach an RNN to evolve about a Lorenz-shaped manifold, and to control its evolution about a translated, transformed, and bifurcated continua of such manifolds. Our approach contributes to prior work on artificial neural networks in three significant ways [25, 32, 33, 35]. First, we provide a means by which a neural system can learn continuous interpolated and extrapolated modifications, along with discontinuous bifurcations, of its own representation solely through examples. Second, the learned manifolds are spatially and temporally complex, allowing for potential extensions to learning modifications of time series data such as speech or music with a structured yet unpredictable evolution. Third, we use a randomly generated and arbitrarily connected network that does not need to be artificially engineered to preserve invariance or manipulate information [25].

One of the main limitations of this work is the lack of a clear mechanism of how the network connectivity ultimately stabilizes the chaotic manifold. Much progress has been made in tackling this limitation, both by exercising theoretical concepts of generalized synchronization [36], and by developing tools for controlling chaos [37]. However, there is insufficient knowledge to guarantee that a set of training and reservoir parameters will always successfully teach the desired computation. Similarly, we are unable to specify exactly how far to space the training examples for the feedback reservoir to successfully learn the linear relationships between the differential of the reservoir states and the control parameter.

A particularly promising area for future work is related to the simple quadratic form of the reservoir. Because all of these results are obtained by driving our reservoir in the quadratic regime, the same results should hold for common neural mass models, such as the Wilson-Cowan model [38]. Hence, these results may provide a unifying framework for learning and computing in dynamical neural models. Additionally, these results provide a basis for exploring more complex computations, such as inferring bifurcations in experimental data, and testing the reservoir’s “imagination” in reconstructing more complex chaotic manifolds using incomplete data. Finally, and perhaps most astonishingly, the reservoir’s ability to accurately reconstruct the full nonlinear geometry of the bifurcated Lorenz manifold after only observing pre-bifurcation data implies that it is not only imitating examples, but actually inferring higher-order nonlinear structure. This work therefore provides a starting point for exploring exactly how higher-order structure is learned by neural systems.

226 IX. ACKNOWLEDGMENTS

227 We are thankful for the insightful feedback and comments from Harang Ju and Keith
228 Wiley. We gratefully acknowledge support from the John D. and Catherine T. MacArthur
229 Foundation, the Alfred P. Sloan Foundation, the ISI Foundation, the Paul Allen Founda-
230 tion, the Army Research Laboratory (No. W911NF-10-2-0022), the Army Research Office
231 (Nos. Bassett-W911NF-14-1-0679, Grafton-W911NF-16-1-0474, and DCIST-W911NF-17-2-
232 0181), the Office of Naval Research (ONR), the National Institute of Mental Health (Nos. 2-
233 R01-DC-009209-11, R01-MH112847, R01-MH107235, and R21-MH-106799), the National
234 Institute of Child Health and Human Development (No. 1R01HD086888-01), National In-
235 stitute of Neurological Disorders and Stroke (No. R01 NS099348), and the National Science
236 Foundation (NSF) (Nos. DGE-1321851, BCS-1441502, BCS-1430087, NSF PHY-1554488,
237 and BCS-1631550). The content is solely the responsibility of the authors and does not
238 necessarily represent the official views of any of the funding agencies.

239 X. CITATION DIVERSITY STATEMENT

240 Recent work in several fields of science has identified a bias in citation practices such
241 that papers from women and other minorities are under-cited relative to other papers in the
242 field [39]. Here we sought to proactively consider choosing references that reflect the diver-
243 sity of our field in thought, form of contribution, gender, and other factors. We classified
244 gender based on the first names of the first and last authors, with possible combinations
245 including male/male, male/female, female/male, and female/female. We regret that our
246 current methodology is limited to consideration of gender as a binary variable. Excluding
247 self-citations to the first and senior authors of our present paper, the references contain 50%
248 male/male, 23.5% male/female, 11.8% female/male, and 14.7% female/female categoriza-
249 tions. We look forward to future work that will help us to better understand how to support
250 equitable practices in science.

251 **XI. REFERENCES**

- 252 [1] Nvidia. *Nvidia V100 Tensor Core GPU* (2020). URL [https://images.nvidia.com/
253 content/technologies/volta/pdf/volta-v100-datasheet-update-us-1165301-r5.pdf](https://images.nvidia.com/content/technologies/volta/pdf/volta-v100-datasheet-update-us-1165301-r5.pdf).
- 254 [2] Intel Corporation. *8th and 9th Generation Intel Core Processor Families, Volume 1 of 2*
255 (2019). URL [https://www.intel.com/content/www/us/en/products/docs/processors/
256 core/8th-gen-core-family-datasheet-vol-1.html](https://www.intel.com/content/www/us/en/products/docs/processors/core/8th-gen-core-family-datasheet-vol-1.html). Rev. 003.
- 257 [3] von Neumann, J. First draft of a report on the EDVAC. *IEEE Annals of the History of*
258 *Computing* **15**, 27–75 (1993).
- 259 [4] Alglave, J. *et al.* The semantics of power and ARM multiprocessor machine code. In *Pro-*
260 *ceedings of the 4th workshop on Declarative aspects of multicore programming - DAMP '09*,
261 13 (ACM Press, New York, New York, USA, 2008).
- 262 [5] Zhang, Z., Jiao, Y.-Y. & Sun, Q.-Q. Developmental maturation of excitation and inhibition
263 balance in principal neurons across four layers of somatosensory cortex. *Neuroscience* **174**,
264 10–25 (2011).
- 265 [6] Faulkner, R. L. *et al.* Development of hippocampal mossy fiber synaptic outputs by new
266 neurons in the adult brain. *Proceedings of the National Academy of Sciences* **105**, 14157–
267 14162 (2008).
- 268 [7] Dunn, F. A. & Wong, R. O. L. Diverse Strategies Engaged in Establishing Stereotypic Wiring
269 Patterns among Neurons Sharing a Common Input at the Visual System’s First Synapse.
270 *Journal of Neuroscience* **32**, 10306–10317 (2012).
- 271 [8] Craik, F. I. & Bialystok, E. Cognition through the lifespan: mechanisms of change. *Trends*
272 *in Cognitive Sciences* **10**, 131–138 (2006).
- 273 [9] Tacchetti, A., Isik, L. & Poggio, T. A. Invariant Recognition Shapes Neural Representations
274 of Visual Input. *Annual Review of Vision Science* **4**, 403–422 (2018).
- 275 [10] Moser, E. I., Kropff, E. & Moser, M.-B. Place Cells, Grid Cells, and the Brain’s Spatial
276 Representation System. *Annual Review of Neuroscience* **31**, 69–89 (2008).
- 277 [11] Ifft, P. J., Shokur, S., Li, Z., Lebedev, M. A. & Nicolelis, M. A. L. A Brain-Machine Interface
278 Enables Bimanual Arm Movements in Monkeys. *Science Translational Medicine* **5**, 210ra154–

- 279 210ra154 (2013).
- 280 [12] Sainath, T. N. *et al.* Deep Convolutional Neural Networks for Large-scale Speech Tasks.
281 *Neural Networks* **64**, 39–48 (2015).
- 282 [13] Jarrell, T. A. *et al.* The Connectome of a Decision-Making Neural Network. *Science* **337**,
283 437–444 (2012).
- 284 [14] Lee, J. & Tashev, I. High-level feature representation using recurrent neural network for
285 speech emotion recognition. In *Proceedings of the Annual Conference of the International*
286 *Speech Communication Association, INTERSPEECH*, vol. 2015-Janua, 1537–1540 (2015).
- 287 [15] Wang, J., Narain, D., Hosseini, E. A. & Jazayeri, M. Flexible timing by temporal scaling of
288 cortical responses. *Nature Neuroscience* **21**, 102–110 (2018).
- 289 [16] Weber, M., Maia, P. D. & Kutz, J. N. Estimating Memory Deterioration Rates Following
290 Neurodegeneration and Traumatic Brain Injuries in a Hopfield Network Model. *Frontiers in*
291 *Neuroscience* **11** (2017).
- 292 [17] Burak, Y. & Fiete, I. R. Accurate Path Integration in Continuous Attractor Network Models
293 of Grid Cells. *PLoS Computational Biology* **5**, e1000291 (2009).
- 294 [18] Yoon, K. *et al.* Specific evidence of low-dimensional continuous attractor dynamics in grid
295 cells. *Nature Neuroscience* **16**, 1077–1084 (2013).
- 296 [19] Hegarty, M. Mechanical reasoning by mental simulation. *Trends in Cognitive Sciences* **8**,
297 280–285 (2004).
- 298 [20] Kubricht, J. R., Holyoak, K. J. & Lu, H. Intuitive Physics: Current Research and Controversies.
299 *Trends in Cognitive Sciences* **21**, 749–759 (2017).
- 300 [21] Pfeiffer, B. E. & Foster, D. J. Hippocampal place-cell sequences depict future paths to re-
301 membered goals. *Nature* **497**, 74–79 (2013).
- 302 [22] Gold, J. I. & Shadlen, M. N. The Neural Basis of Decision Making. *Annual Review of*
303 *Neuroscience* **30**, 535–574 (2007).
- 304 [23] Strogatz, S. H. *Nonlinear Dynamics and Chaos* (Perseus Books, 1994), 1 edn.
- 305 [24] Yang, J., Wang, L., Wang, Y. & Guo, T. A novel memristive Hopfield neural network with
306 application in associative memory. *Neurocomputing* **227**, 142–148 (2017).
- 307 [25] Wu, S., Wong, K. Y. M., Fung, C. C. A., Mi, Y. & Zhang, W. Continuous Attractor
308 Neural Networks: Candidate of a Canonical Model for Neural Information Representation.
309 *F1000Research* **5**, 156 (2016).

- 310 [26] Graves, A. *et al.* Hybrid computing using a neural network with dynamic external memory.
311 *Nature* **538**, 471–476 (2016).
- 312 [27] Carroll, J. M. Letter knowledge precipitates phoneme segmentation, but not phoneme invari-
313 ance. *Journal of Research in Reading* **27**, 212–225 (2004).
- 314 [28] Fee, M. S. & Scharff, C. The Songbird as a Model for the Generation and Learning of Complex
315 Sequential Behaviors. *ILAR Journal* **51**, 362–377 (2010).
- 316 [29] Donnay, G. F., Rankin, S. K., Lopez-Gonzalez, M., Jiradejvong, P. & Limb, C. J. Neural
317 Substrates of Interactive Musical Improvisation: An fMRI Study of ‘Trading Fours’ in Jazz.
318 *PLoS ONE* **9**, e88665 (2014).
- 319 [30] Qiao, J., Li, F., Han, H. & Li, W. Growing Echo-State Network With Multiple Subreservoirs.
320 *IEEE Transactions on Neural Networks and Learning Systems* **28**, 391–404 (2017).
- 321 [31] Lorenz, E. N. Deterministic Nonperiodic Flow. *Journal of the Atmospheric Sciences* **20**,
322 130–141 (1963).
- 323 [32] Jaeger, H. The “echo state” approach to analysing and training recurrent neural networks
324 – with an Erratum note. *GMD Report* **1**, 1–47 (2010).
- 325 [33] Sussillo, D. & Abbott, L. Generating Coherent Patterns of Activity from Chaotic Neural
326 Networks. *Neuron* **63**, 544–557 (2009).
- 327 [34] Slowik, R. Inverses and Determinants of Toeplitz-Hessenberg Matrices. *Taiwanese Journal of*
328 *Mathematics* **22**, 901–908 (2018).
- 329 [35] Seung, H. S. Learning continuous attractors in recurrent networks. In *Advances in Neural*
330 *Information Processing Systems*, 654–660 (MIT Press, 1998).
- 331 [36] Rulkov, N. F., Sushchik, M. M., Tsimring, L. S. & Abarbanel, H. D. I. Generalized synchro-
332 nization of chaos in directionally coupled chaotic systems. *Physical Review E* **51**, 980–994
333 (1995).
- 334 [37] Ott, E., Grebogi, C. & Yorke, J. A. Controlling chaos. *Physical Review Letters* **64**, 1196–1199
335 (1990).
- 336 [38] Wilson, H. R. & Cowan, J. D. Excitatory and Inhibitory Interactions in Localized Populations
337 of Model Neurons. *Biophysical Journal* **12**, 1–24 (1972).
- 338 [39] Dworkin, J. D. *et al.* The extent and drivers of gender imbalance in neuroscience reference
339 lists. *bioRxiv* (2020).

Supplement to “Teaching Recurrent Neural Networks to Modify Chaotic Memories by Example”

Jason Z. Kim

Department of Bioengineering, University of Pennsylvania, Philadelphia, PA, 19104

Zhixin Lu

Department of Bioengineering, University of Pennsylvania, Philadelphia, PA, 19104

Erfan Nozari

*Department of Electrical and Systems Engineering,
University of Pennsylvania, Philadelphia, PA, 19104*

George J. Pappas

*Department of Electrical and Systems Engineering,
University of Pennsylvania, Philadelphia, PA, 19104*

Danielle S. Bassett

*Departments of Bioengineering, Physics & Astronomy,
Electrical & Systems Engineering, Neurology, and Psychiatry,
University of Pennsylvania, Philadelphia, PA, 19104
Santa Fe Institute, Santa Fe, NM 87501 and
To whom correspondence should be addressed: dsb@seas.upenn.edu*

(Dated: May 3, 2020)

CONTENTS

I. Methods	3
A. Reservoir dynamics	3
B. Derivation of quadratic reservoir	5
C. Simulation parameters	8
1. Global parameters	8
2. Lorenz training data parameters	8
3. Reservoir	8
D. Simulation method	9
E. Training	11
F. Training maps the fixed point to 0	12
G. Truncation of the block-Hessenberg matrix	13
H. Summary	15
II. Results	16
A. Translation in multiple directions	16
B. Different types of transformations	17
References	18

1 I. METHODS

2 In this section, we describe additional details about the methods and simulations used
3 in the main text. We begin with a more thorough overview of reservoir dynamics and their
4 derivation, followed by specific details of the numerical simulations.

5 A. Reservoir dynamics

6 The reservoir computing framework is a general scheme by which a nonlinear dynamical
7 system (the reservoir) is driven by some input, and a simple linear readout of the reservoir
8 states is trained [1]. The reservoir consists of N neural units, where each unit i has a
9 real-valued level of activity over time, $r_i(t)$. We collect this activity into an N -dimensional
10 column vector

$$\mathbf{r}(t) = \begin{bmatrix} r_1(t) \\ r_2(t) \\ \vdots \\ r_N(t) \end{bmatrix},$$

11 that we refer to as the *reservoir state*. These reservoir states are driven by some input time
12 series of M inputs $x_1(t), x_2(t), \dots, x_M(t)$, that we collect into the input vector

$$\mathbf{x}(t) = \begin{bmatrix} x_1(t) \\ x_2(t) \\ \vdots \\ x_M(t) \end{bmatrix}.$$

13 In our framework, we add a set of K control inputs c_1, \dots, c_K that we collect into the control
14 vector

$$\mathbf{c} = \begin{bmatrix} c_1 \\ c_2 \\ \vdots \\ c_K \end{bmatrix}.$$

15 For continuous time systems ($t \in \mathbb{R}_{\geq 0}$), a typical equation for the time-evolution of a
16 reservoir consists of a nonlinear (usually sigmoidal [1]) transformation \mathbf{g} on a linear sum of

17 all inputs and states written as

$$\frac{1}{\gamma}\dot{\mathbf{r}}(t) = -\mathbf{r}(t) + \mathbf{g}(A\mathbf{r}(t) + B\mathbf{x}(t) + C\mathbf{c} + \mathbf{d}),$$

18 where $\dot{\mathbf{r}}(t)$ represents the time derivative [2, 3], A is a real-valued matrix of dimension $N \times N$,
 19 B is a real-valued matrix of dimension $N \times M$, C is a real-valued matrix of dimension $N \times K$,
 20 and \mathbf{d} is a constant bias vector of dimension $N \times 1$. We can write the dynamics for each
 21 reservoir state, $r_i(t)$, as

$$\frac{1}{\gamma}\dot{r}_i(t) = -r_i(t) + g_i \left(\sum_{n=1}^N A_{in}r_n(t) + \sum_{m=1}^M B_{im}x_m(t) + \sum_{k=1}^K C_{ik}c_k + d_i \right).$$

22 If we write A_{i*} , B_{i*} , and C_{i*} as the i -th row of matrices A , B , and C , respectively, we can
 23 write this equation more concisely as

$$\frac{1}{\gamma}\dot{r}_i(t) = -r_i(t) + g_i (A_{i*}\mathbf{r}(t) + B_{i*}\mathbf{x}(t) + C_{i*}\mathbf{c} + d_i). \quad (1)$$

24 We begin by observing that the reservoir states are evolved according to some prede-
 25 termined input $\mathbf{x}(t)$ and control input \mathbf{c} to generate the reservoir state time series $\mathbf{r}(t)$.
 26 Next, linear combinations of the reservoir state are taken to approximate the input $\mathbf{x}(t)$ by
 27 minimizing the matrix 2-norm of the difference in the numerical time series (see Sec. I E)

$$\|W\mathbf{r}(t) - \mathbf{x}(t)\|_2,$$

28 where W is the real valued matrix of dimension $M \times N$ that is trained. After training, we
 29 perform feedback by replacing the inputs $\mathbf{x}(t)$ with the trained outputs $W\mathbf{r}(t)$ to yield the
 30 feedback dynamics

$$\frac{1}{\gamma}\dot{\mathbf{r}}'(t) = -\mathbf{r}'(t) + \mathbf{g}(A\mathbf{r}'(t) + BW\mathbf{r}'(t) + C\mathbf{c} + \mathbf{d}),$$

31 and by factoring the term $R = A + BW$, we obtain

$$\frac{1}{\gamma}\dot{\mathbf{r}}'(t) = -\mathbf{r}'(t) + \mathbf{g}(R\mathbf{r}'(t) + C\mathbf{c} + \mathbf{d}).$$

32 This feedback equation is written element-wise as

$$\frac{1}{\gamma}\dot{r}'_i(t) = -r'_i(t) + g_i \left(\sum_{n=1}^N R_{in}r'_n(t) + \sum_{k=1}^K C_{ik}c_k + d_i \right).$$

33 We note that R is an $N \times N$ matrix.

34

B. Derivation of quadratic reservoir

35

36

37

38

39

40

41

42

43

44

While the reservoir computing framework often uses a specific nonlinear sigmoid function for \mathbf{g} , our goal is to find principles of learning relevant to a broad range of functional forms of \mathbf{g} . To achieve this goal, we study the reservoir in the weakly nonlinear regime. By deriving insights in this regime, we aim to make statements about dynamical systems with many different forms of \mathbf{g} as long they are driven in the same regime. By weakly nonlinear, we mean the *quadratic* regime, where the reservoir evolves nearby some constant stable fixed point attractor \mathbf{r}^* . This regime is explicitly encoded by taking the second-order Taylor series expansion of the dynamics about a steady state in all of the inputs \mathbf{r}^* , \mathbf{x}^* , \mathbf{c}^* . For notational convenience, we write $\delta\mathbf{r} = \mathbf{r} - \mathbf{r}^*$, $\delta\mathbf{x} = \mathbf{x} - \mathbf{x}^*$, and $\delta\mathbf{c} = \mathbf{c} - \mathbf{c}^*$, and also omit the notation of time dependence, (t). If we write the full dynamics from Eq. 1 as

$$\frac{1}{\gamma}\dot{r}_i = f_i(\mathbf{r}, \mathbf{x}, \mathbf{c}) = -r_i + g_i(A_{i*}\mathbf{r} + B_{i*}\mathbf{x} + C_{i*}\mathbf{c} + d_i),$$

45

then the Taylor series expansion to second order contains terms

$$T_{i,0} = f_i|_{\mathbf{r}=\mathbf{r}^*, \mathbf{x}=\mathbf{x}^*, \mathbf{c}=\mathbf{c}^*}$$

$$T_{i,1} = \nabla_{\mathbf{r}, \mathbf{x}, \mathbf{c}} f_i|_{\mathbf{r}=\mathbf{r}^*, \mathbf{x}=\mathbf{x}^*, \mathbf{c}=\mathbf{c}^*}$$

$$T_{i,2} = \nabla_{\mathbf{r}, \mathbf{x}, \mathbf{c}}^2 f_i|_{\mathbf{r}=\mathbf{r}^*, \mathbf{x}=\mathbf{x}^*, \mathbf{c}=\mathbf{c}^*},$$

46

where ∇ is the gradient operator with respect to the subscripted variables

$$\begin{aligned} \nabla_{\mathbf{r}, \mathbf{x}, \mathbf{c}} &= \left[\nabla_{\mathbf{r}}, \nabla_{\mathbf{x}}, \nabla_{\mathbf{c}} \right] \\ &= \left[\frac{\partial}{\partial r_1}, \dots, \frac{\partial}{\partial r_N}, \frac{\partial}{\partial x_1}, \dots, \frac{\partial}{\partial x_M}, \frac{\partial}{\partial c_1}, \dots, \frac{\partial}{\partial c_K} \right], \end{aligned}$$

47

yielding a vector of partial derivatives, and ∇^2 yields a matrix of all pairwise second partial

48

derivatives. Then the quadratic dynamics become

$$\frac{1}{\gamma}\delta\dot{r}_i \approx T_{i,0} + T_{i,1} \begin{bmatrix} \delta\mathbf{r} \\ \delta\mathbf{x} \\ \delta\mathbf{c} \end{bmatrix} + \frac{1}{2} \begin{bmatrix} \delta\mathbf{r}^\top & \delta\mathbf{x}^\top & \delta\mathbf{c}^\top \end{bmatrix} T_{i,2} \begin{bmatrix} \delta\mathbf{r} \\ \delta\mathbf{x} \\ \delta\mathbf{c} \end{bmatrix}.$$

49

As we are evaluating the dynamics about a fixed point, the reservoir does not change its

50

state at this point, such that $f_i|_{\mathbf{r}=\mathbf{r}^*, \mathbf{x}=\mathbf{x}^*, \mathbf{c}=\mathbf{c}^*} = 0$. Hence the term

$$T_{i,0} = 0$$

51 vanishes. The next term, $T_{i,1}$, is a linear approximation of the dynamics f_i

$$\begin{aligned} T_{i,1} &= \nabla_{\mathbf{r},\mathbf{x},\mathbf{c}}(-r_i) + \nabla_{\mathbf{r},\mathbf{x},\mathbf{c}}g_i(A_{i*}\mathbf{r} + B_{i*}\mathbf{x} + C_{i*}\mathbf{c} + d_i) \\ &= [0, \dots, 0, -1, 0, \dots, 0] + u_i [A_{i*}, B_{i*}, C_{i*}], \end{aligned}$$

52 where $u_i = \left. \frac{\partial g_i}{\partial(\mathbf{r},\mathbf{x},\mathbf{c})} \right|_{\mathbf{r}^*,\mathbf{x}^*,\mathbf{c}^*}$ is the evaluation of the first derivative of g_i at the fixed point,
53 and the subsequent term $T_{i,2}$ approximates the quadratic curvature of f_i as follows:

$$\begin{aligned} T_{i,2} &= \nabla_{\mathbf{r},\mathbf{x},\mathbf{c}}^2 f_i |_{\mathbf{r}=\mathbf{r}^*,\mathbf{x}=\mathbf{x}^*,\mathbf{c}=\mathbf{c}^*} \\ &= 2v_i \begin{bmatrix} A_{i*}^\top \\ B_{i*}^\top \\ C_{i*}^\top \end{bmatrix} [A_{i*}, B_{i*}, C_{i*}], \end{aligned}$$

54 where $v_i = \frac{1}{2} \left. \frac{\partial^2 g_i}{\partial(\mathbf{r},\mathbf{x},\mathbf{c})^2} \right|_{\mathbf{r}^*,\mathbf{x}^*,\mathbf{c}^*}$ is half of the evaluation of the second derivative of g_i at the
55 fixed point. Substituting these values back into the quadratic dynamics, we obtain

$$\frac{1}{\gamma} \delta \dot{r}_i \approx -\delta r_i + u_i [A_{i*}, B_{i*}, C_{i*}] \begin{bmatrix} \delta \mathbf{r} \\ \delta \mathbf{x} \\ \delta \mathbf{c} \end{bmatrix} + v_i [\delta \mathbf{r}^\top \ \delta \mathbf{x}^\top \ \delta \mathbf{c}^\top] \begin{bmatrix} A_{i*}^\top \\ B_{i*}^\top \\ C_{i*}^\top \end{bmatrix} [A_{i*}, B_{i*}, C_{i*}] \begin{bmatrix} \delta \mathbf{r} \\ \delta \mathbf{x} \\ \delta \mathbf{c} \end{bmatrix},$$

56 and we notice that

$$[\delta \mathbf{r}^\top \ \delta \mathbf{x}^\top \ \delta \mathbf{c}^\top] \begin{bmatrix} A_{i*}^\top \\ B_{i*}^\top \\ C_{i*}^\top \end{bmatrix} = [A_{i*}, B_{i*}, C_{i*}] \begin{bmatrix} \delta \mathbf{r} \\ \delta \mathbf{x} \\ \delta \mathbf{c} \end{bmatrix},$$

57 to yield

$$\frac{1}{\gamma} \delta \dot{r}_i \approx -\delta r_i + u_i [A_{i*}, B_{i*}, C_{i*}] \begin{bmatrix} \delta \mathbf{r} \\ \delta \mathbf{x} \\ \delta \mathbf{c} \end{bmatrix} + v_i \left([A_{i*}, B_{i*}, C_{i*}] \begin{bmatrix} \delta \mathbf{r} \\ \delta \mathbf{x} \\ \delta \mathbf{c} \end{bmatrix} \right)^2,$$

58 which can be rewritten as

$$\frac{1}{\gamma} \delta \dot{r}_i \approx -\delta r_i + u_i (A_{i*} \delta \mathbf{r} + B_{i*} \delta \mathbf{x} + C_{i*} \delta \mathbf{c}) + v_i (A_{i*} \delta \mathbf{r} + B_{i*} \delta \mathbf{x} + C_{i*} \delta \mathbf{c})^2.$$

59 Compiling the dynamics of all reservoir nodes \mathbf{r} , we write the compact vector form of the
60 dynamics as

$$\frac{1}{\gamma} \delta \dot{\mathbf{r}} = -\delta \mathbf{r} + U(A \delta \mathbf{r} + B \delta \mathbf{x} + C \delta \mathbf{c}) + V(A \delta \mathbf{r} + B \delta \mathbf{x} + C \delta \mathbf{c})^2,$$

61 where U and V are diagonal matrices where the i -th elements are u_i and v_i obtained by eval-
62 uating the first and second derivatives of g_i , respectively. To avoid making any assumptions
63 about the operating point of the input states or control inputs, we linearize about $\mathbf{x}^* = \mathbf{0}$
64 and $\mathbf{c}^* = \mathbf{0}$. Further, we notice that $\delta\dot{\mathbf{r}} = \frac{d}{dt}(\mathbf{r} - \mathbf{r}^*) = \dot{\mathbf{r}}$. Hence, the above vector form of
65 the equation becomes

$$\frac{1}{\gamma}\delta\dot{\mathbf{r}} = -\delta\mathbf{r} + U(A\delta\mathbf{r} + B\mathbf{x} + C\mathbf{c}) + V(A\delta\mathbf{r} + B\mathbf{x} + C\mathbf{c})^2. \quad (2)$$

66 Importantly, we note that the elements of U and V are not allowed to arbitrarily be
67 any value. Instead, their values depend on the first and second derivatives of the activation
68 function \mathbf{g} evaluated at the fixed points \mathbf{r}^* , \mathbf{x}^* , and \mathbf{c}^* . For the sake of remaining relevant
69 to the existing literature that frequently uses the hyperbolic tangent function \tanh [1], we
70 will restrict the values of U and V . First, we note that at the fixed point, we have

$$\mathbf{0} = -\mathbf{r}^* + \mathbf{g}(A\mathbf{r}^* + B\mathbf{x}^* + C\mathbf{c}^*).$$

71 Recall that we evaluate our functions at $\mathbf{x}^* = \mathbf{0}$ and $\mathbf{c}^* = \mathbf{0}$, such that $\mathbf{g}(A\mathbf{r}^*) = \mathbf{r}^*$,
72 regardless of the form of \mathbf{g} . Next, we consider the specific activation function

$$\mathbf{g}(\mathbf{r}, \mathbf{x}, \mathbf{c}) = \tanh(A\mathbf{r} + B\mathbf{x} + C\mathbf{c} + \mathbf{d}),$$

73 and evaluate its first derivative at \mathbf{r}^* , $\mathbf{x}^* = \mathbf{0}$, $\mathbf{c}^* = \mathbf{0}$ to yield

$$d\mathbf{g}_{\mathbf{r}^*, \mathbf{x}^*=\mathbf{0}, \mathbf{c}^*=\mathbf{0}} = \mathbf{1} - \tanh(A\mathbf{r}^*)^2 = \mathbf{1} - \mathbf{r}^{*2}, \quad (3)$$

74 where $\mathbf{1}$ is an N -dimensional vector of ones, and the square notation of the vector implies an
75 element-wise square. Hence, U is a diagonal matrix where the i -th entry is $1 - r_i^{*2}$. Finally,
76 we take the second derivative

$$d^2\mathbf{g}_{\mathbf{r}^*, \mathbf{x}^*=\mathbf{0}, \mathbf{c}^*=\mathbf{0}} = -2(\tanh(A\mathbf{r}^*) - \tanh(A\mathbf{r}^*)^3) = 2(\mathbf{r}^{*3} - \mathbf{r}^*), \quad (4)$$

77 such that the i -th diagonal element of V is given by $r_i^{*3} - r_i^*$. Hence, for the quadratic
78 approximation of \tanh , it is sufficient to specify a fixed point \mathbf{r}^* to fully determine the
79 matrices U and V .

80

C. Simulation parameters

81

For all simulations in the main text of the paper, we used the following parameter choices:

82

1. Global parameters

83

- simulation time step: $\Delta t = 0.001$.

84

2. Lorenz training data parameters

85

- dynamical equation:

86

$$\dot{x}_1 = \sigma(x_2 - x_1) \qquad \dot{x}_2 = x_1(\rho - x_3) - x_2 \qquad \dot{x}_3 = x_1x_2 - \beta x_3.$$

87

- parameters: $\sigma = 10, \beta = 8/3, \rho = 28$ (except in the bifurcation example).

88

- uniform random initial conditions: $x_1, x_2, x_3 \in [0, 10]$.

89

- throwaway simulation time (per attractor): $T_{\text{waste}} = 20$.

90

- training simulation time (per attractor): $T_{\text{train}} = 200$.

91

- translation training shift: $P = \begin{bmatrix} 1 \\ 0 \\ 0 \end{bmatrix}$.

92

- transformation training stretch: $P = \begin{bmatrix} -.012 & 0 & 0 \\ 0 & 0 & 0 \\ 0 & 0 & 0 \end{bmatrix}$.

93

3. Reservoir

94

- dynamical equation: $\frac{1}{\gamma}\dot{\mathbf{r}} = -\delta\mathbf{r} + U(A\delta\mathbf{r} + B\mathbf{x} + C\mathbf{c}) + V(A\delta\mathbf{r} + B\mathbf{x} + C\mathbf{c})^2$.

95

- reservoir initial condition: $\mathbf{r}(0) = \mathbf{0}$.

96

- adjacency matrix A has 10% binary density. We begin with matrix \tilde{A} where each nonzero element is drawn from a uniform random distribution $\tilde{A}_{ij} \in [-1, 1]$. Then the

97

98 matrix is normalized such that $A = 0.95 \frac{\tilde{A}}{\text{real}(\lambda_{\max})}$, where λ_{\max} is the eigenvalue with
 99 the largest real value. For a *tanh* activation function, this normalization is used to
 100 ensure the echo-state property in discrete time reservoir systems [2].

- 101 • number of reservoir neurons: $N = 300$.
- 102 • time constant: $\gamma = 100$.
- 103 • fixed point: each element was drawn from a random uniform distribution $r_i^* \in$
 104 $[-1, -0.8] \cup [0.8, 1]$.
- 105 • data input matrix: every row i of B has one non-zero element at index j . This
 106 index is chosen uniformly at random ($Pr(j = 1) = \dots = Pr(j = M)$). For examples
 107 involving translations and transformations, the value of the element is drawn uniformly
 108 from $B_{ij} \in [-0.004, 0.004]$. For examples involving bifurcations, the magnitude of
 109 the observed data is much smaller (local to the stable fixed point, instead of the
 110 full chaotic attractor manifold), and therefore the element is drawn uniformly from
 111 $B_{ij} \in [-0.04, 0.04]$.
- 112 • control input matrix: every row i of C has one non-zero element at index j . This index
 113 is chosen uniformly and randomly ($Pr(j = 1) = \dots = Pr(j = K)$), and the value of
 114 the element is drawn uniformly from $C_{ij} \in [-0.002, 0.002]$.

115 D. Simulation method

To simulate both the input and reservoir dynamics, we used a 4-th order Runge-Kutta numerical integration. For the dynamics of the Lorenz attractor,

$$\dot{\mathbf{x}} = \mathbf{f}(\mathbf{x}),$$

116 the Runge-Kutta computes the following values

$$\begin{aligned} k_{x1} &= \Delta t \cdot \mathbf{f}(\mathbf{x}(t)) \\ k_{x2} &= \Delta t \cdot \mathbf{f}\left(\mathbf{x}(t) + \frac{k_{x1}}{2}\right) \\ k_{x3} &= \Delta t \cdot \mathbf{f}\left(\mathbf{x}(t) + \frac{k_{x2}}{2}\right) \\ k_{x4} &= \Delta t \cdot \mathbf{f}(\mathbf{x}(t) + k_{x3}), \end{aligned}$$

117 and evolves the state forward using

$$\mathbf{x}(t + \Delta t) = \mathbf{x}(t) + \frac{1}{6}(k_{x1} + 2k_{x2} + 2k_{x3} + k_{x4}).$$

118 The simulation of the reservoir dynamics requires more careful analysis, because it is a
119 system driven by external inputs. For the original reservoir dynamics given by Eq. 2

$$\frac{1}{\gamma}\dot{\mathbf{r}} = \mathbf{f}(\mathbf{r}, \mathbf{x}, \mathbf{c}) = -\delta\mathbf{r} + U(A\delta\mathbf{r} + B\mathbf{x} + C\mathbf{c}) + V(A\delta\mathbf{r} + B\mathbf{x} + C\mathbf{c})^2,$$

120 the algorithm to update the reservoir states is given by

$$\begin{aligned} k_{r1} &= \Delta t \cdot \mathbf{f}(\mathbf{r}(t), \mathbf{x}(t), \mathbf{c}(t)) \\ k_{r2} &= \Delta t \cdot \mathbf{f}\left(\mathbf{r}(t) + \frac{k_{r1}}{2}, \mathbf{x}(t) + \frac{k_{x1}}{2}, \mathbf{c}(t) + \frac{k_{c1}}{2}\right) \\ k_{r3} &= \Delta t \cdot \mathbf{f}\left(\mathbf{r}(t) + \frac{k_{r2}}{2}, \mathbf{x}(t) + \frac{k_{x2}}{2}, \mathbf{c}(t) + \frac{k_{c2}}{2}\right) \\ k_{r4} &= \Delta t \cdot \mathbf{f}(\mathbf{r}(t) + k_{r3}, \mathbf{x}(t) + k_{x3}, \mathbf{c}(t) + k_{c3}), \end{aligned}$$

121 and the reservoir state evolves forward according to

$$\mathbf{r}(t + \Delta t) = \mathbf{r}(t) + \frac{1}{6}(k_{r1} + 2k_{r2} + 2k_{r3} + k_{r4}).$$

122 Hence, when we simulate the Lorenz state $\mathbf{x}(t)$, we also save the corresponding values
123 k_{x1}, \dots, k_{x3} to use in the reservoir update algorithm. Finally, we note that in our simulations,
124 we slowly vary the control input $\mathbf{c}(t)$ over time, requiring us to determine the trajectory of
125 $\mathbf{c}(t)$ beforehand. However, we require a differential equation that generated $\mathbf{c}(t)$ to solve for
126 the final parameters k_{c1}, \dots, k_{c4} . We assume the differential equations that generate \mathbf{c} are
127 constant, such that between time t and $t + \Delta t$, the rate of change of $\mathbf{c}(t)$ is given by

$$\dot{\mathbf{c}}(t) = \mathbf{f}(\mathbf{c}(t)) = \frac{\mathbf{c}(t + \Delta t) - \mathbf{c}(t)}{\Delta t}.$$

128 Such dynamics yield the parameters

$$\begin{aligned} k_{c1} &= \Delta t \cdot \mathbf{f}(\mathbf{c}(t)) = \mathbf{c}(t + \Delta t) - \mathbf{c}(t) \\ k_{c2} &= \Delta t \cdot \mathbf{f}\left(\mathbf{c}(t) + \frac{k_{c1}}{2}\right) = \Delta t \cdot \mathbf{f}\left(\frac{\mathbf{c}(t + \Delta t) + \mathbf{c}(t)}{2}\right) = \mathbf{c}(t + \Delta t) - \mathbf{c}(t) \\ k_{c3} &= \Delta t \cdot \mathbf{f}\left(\mathbf{c}(t) + \frac{k_{c2}}{2}\right) = \Delta t \cdot \mathbf{f}\left(\frac{\mathbf{c}(t + \Delta t) + \mathbf{c}(t)}{2}\right) = \mathbf{c}(t + \Delta t) - \mathbf{c}(t). \end{aligned}$$

129 The same integration is used with feedback where $\frac{1}{\gamma}\dot{\mathbf{r}} = \mathbf{f}(\mathbf{r}, \mathbf{c}) = -\delta\mathbf{r} + U(R\delta\mathbf{r} + C\mathbf{c}) +$
130 $V(R\delta\mathbf{r} + C\mathbf{c})^2$.

131 **E. Training**

132 Using the dynamical equations and RK4 integration scheme, we first generated the Lorenz
 133 attractor training inputs $\mathbf{x}(t)$. Each of the single direction translation and transformation
 134 examples described in the main text used four Lorenz attractor inputs. The first was the
 135 original Lorenz time series $\mathbf{x}(t)$, and the remaining three were translations or rotations of the
 136 original. Each of these four time series were simulated for $T = T_{\text{waste}} + T_{\text{train}} = 20 + 200 = 220$
 137 time. At a time step of $\Delta t = 0.001$, each time series $\mathbf{x}(t)$ contained $\frac{T}{\Delta t} = 220,000$ simulation
 138 time points, stored in data matrix X_0 for the original attractor. Because we also kept the
 139 4 outputs of the *RK4* numerical integration scheme, the data matrix X_0 had dimensions
 140 variables \times time steps \times RK4 = $3 \times 220,000 \times 4$. With three additional time series for
 141 translation or rotation, X_1, X_2, X_3 , we concatenated the four time series along the second
 142 dimension into the full matrix X with dimension $3 \times 880,000 \times 4$.

143 Using this Lorenz data matrix X , and a corresponding control input data matrix, we
 144 drove the reservoir to generate $\mathbf{r}(t)$, contained in a reservoir data matrix D that was of
 145 size $N = 300 \times 880,000$. For every $\frac{T}{\Delta t} = 220,000$ time steps, we threw away the first
 146 $\frac{T_{\text{waste}}}{\Delta t} = 20,000$ time points, as this simulation allowed both the Lorenz and reservoir systems
 147 to forget their initial conditions. The remaining $\frac{T_{\text{train}}}{\Delta t} = 200,000$ time points of each attractor
 148 were kept for training. This process yields a Lorenz training matrix X_{train} of dimension
 149 $3 \times 800,000$ (as we throw away the RK4 simulation parameters after driving the reservoir),
 150 and a reservoir training matrix D_{train} of dimension $300 \times 800,000$.

151 Finally, we seek a training matrix M of dimension 3×300 that minimizes the matrix
 152 2-norm

$$\|MD_{\text{train}} - X_{\text{train}}\|_2.$$

153 Specifically, we use MATLAB's command `lsqminnorm`, that not only minimizes this norm,
 154 but in the event that multiple solutions exist, also minimizes the norm of M .

155 **F. Training maps the fixed point to 0**

156 Here, we describe a particular but important methodological nuance to the training.
 157 Recall that from Eq. 2, our reservoir evolves according to

$$\frac{1}{\gamma}\dot{\delta\mathbf{r}} = -\delta\mathbf{r} + U(A\delta\mathbf{r} + B\mathbf{x} + C\mathbf{c}) + V(A\delta\mathbf{r} + B\mathbf{x} + C\mathbf{c})^2,$$

158 where $\delta\mathbf{r} = \mathbf{r} - \mathbf{r}^*$. If our training scheme involved approximating the inputs with the
 159 *difference* of the reservoir states $\delta\mathbf{r}$ such that $W\delta\mathbf{r}(t) \approx \mathbf{x}(t)$, then this nuance would be
 160 unnecessary, as the feedback dynamics would take the proper form

$$\begin{aligned} \frac{1}{\gamma}\dot{\mathbf{r}}' &= -\delta\mathbf{r}' + U(A\delta\mathbf{r}' + BW\delta\mathbf{r}' + C\mathbf{c}) + V(A\delta\mathbf{r}' + BW\delta\mathbf{r}' + C\mathbf{c})^2 \\ &= -\delta\mathbf{r}' + U(R\delta\mathbf{r}' + C\mathbf{c}) + V(R\delta\mathbf{r}' + C\mathbf{c})^2. \end{aligned}$$

161 Unfortunately, such a scheme would require the additional assumptions that during training,
 162 the neural system was able to accurately retain knowledge of its fixed point \mathbf{r}^* , and that it
 163 was also able to take the difference of the neural activity with respect to this fixed point in
 164 real time. We avoid these additional assumptions by training on the true reservoir states
 165 such that $W\mathbf{r}(t) \approx \mathbf{x}(t)$, yielding

$$\begin{aligned} \frac{1}{\gamma}\dot{\delta\mathbf{r}}' &= -\delta\mathbf{r}' + U(A\delta\mathbf{r}' + BW\mathbf{r}' + C\mathbf{c}) + V(A\delta\mathbf{r}' + BW\mathbf{r}' + C\mathbf{c})^2 \\ &= -\delta\mathbf{r}' + U(R\delta\mathbf{r}' + BW\mathbf{r}^* + C\mathbf{c}) + V(R\delta\mathbf{r}' + BW\mathbf{r}^* + C\mathbf{c})^2. \end{aligned}$$

166 In both the linear and quadratic terms, we notice an extra and undesired term $BW\mathbf{r}^*$. In
 167 all of our simulations, the training of matrix W actually maps the fixed point to a small
 168 number, such that $W\mathbf{r}^*$ is on the order of 10^{-6} , whereas $W\delta\mathbf{r}(t)$ is on the order of 10^1 .
 169 Hence, the matrix W maps the fixed point to values that are 7 orders of magnitude smaller
 170 than the magnitude of the inputs, such that $W\mathbf{r}'(t) = W\delta\mathbf{r}'(t) + W\mathbf{r}^* \approx W\delta\mathbf{r}'(t)$, thereby
 171 rendering the undesired term $BW\mathbf{r}^*$ effectively negligible.

172 At first, we might be tempted to explain this phenomenon by the fact that the Lorenz
 173 attractor $\mathbf{x}(t)$ is centered around $x_1 = 0$ and $x_2 = 0$. Hence, it would make sense that a
 174 constant fixed point \mathbf{r}^* would map to a value of 0. However, the third coordinate of the
 175 Lorenz system is centered around $x_3 = \rho - 1 = 27$, and yet in our simulations training still
 176 produces an output matrix M that maps the fixed point to 0, even along the x_3 coordinate,
 177 across randomly assigned fixed points \mathbf{r}^* and reservoir parameters A , B , and C .

G. Truncation of the block-Hessenberg matrix

179 To understand the mechanism of learning translations and transformations, we had taken
180 the differential of the reservoir feedback dynamics,

$$(I - KA)dr' + \frac{1}{\gamma}d\dot{r}' = K(BWdr' + Cdc).$$

181 If we take time derivatives of the left-hand side of this equation, we obtain

$$\begin{bmatrix} (I - KA) & \frac{1}{\gamma}I & 0 & 0 & 0 & \dots \\ \downarrow \searrow & & \searrow & & & \\ -\dot{K}A & (I - KA) & \frac{1}{\gamma}I & 0 & 0 & \dots \\ \downarrow \searrow & \downarrow \searrow & \searrow & & & \\ -\ddot{K}A & -2\dot{K}A & (I - KA) & \frac{1}{\gamma}I & 0 & \dots \\ \downarrow \searrow & \downarrow \searrow & \downarrow \searrow & \searrow & & \\ -\dddot{K}A & -3\ddot{K}A & -3\dot{K}A & (I - KA) & \frac{1}{\gamma}I & \dots \\ \vdots & \vdots & \vdots & \vdots & \vdots & \ddots \end{bmatrix} \begin{bmatrix} dr' \\ d\dot{r}' \\ d\ddot{r}' \\ d\ddot{r}' \\ \vdots \end{bmatrix},$$

182 where the element in the i -th row and j -th column has a coefficient

$$p_{i,j} = \binom{i-1}{j-1} \quad \text{for } j \leq i,$$

183 according to Pascal's triangle. For the translation examples, we can write the continued
184 time derivatives of the differential relation as

$$\underbrace{\begin{bmatrix} H_0 & H_{-1} & 0 & 0 & \dots \\ H_1 & H_0 & H_{-1} & 0 & \dots \\ H_2 & 2H_1 & H_0 & H_{-1} & \dots \\ H_3 & 3H_2 & 3H_1 & H_0 & \dots \\ \vdots & \vdots & \vdots & \vdots & \ddots \end{bmatrix}}_J \begin{bmatrix} dr' \\ d\dot{r}' \\ d\ddot{r}' \\ d\ddot{r}' \\ \vdots \end{bmatrix} \approx \begin{bmatrix} K \\ \dot{K} \\ \ddot{K} \\ \ddot{K} \\ \vdots \end{bmatrix} (BP + C)dc,$$

185 where $H_{-1} = \frac{1}{\gamma}I$, $H_0 = I - KA$, and $H_i = -K^{(i)}A$ is the i -th time-derivative of KA . This
186 matrix is a block matrix (each element H is a matrix), and is specifically a block-Hessenberg
187 matrix (zero above the first block-super diagonal). The goal here is to solve for dr' with
188 respect to dc . If we truncate J to a finite-dimensional matrix such that

$$J \simeq \begin{bmatrix} J_{11} & J_{12} \\ J_{21} & J_{22} \end{bmatrix},$$

189 where

$$\begin{aligned}
 J_{11} &= \begin{bmatrix} H_0 \\ H_1 \\ \vdots \\ H_{k-1} \end{bmatrix}, & J_{12} &= \begin{bmatrix} H_{-1}, & 0, & \cdots, & 0 \\ H_0, & H_{-1}, & \cdots, & 0 \\ \vdots & \vdots & \ddots & \vdots \\ p_{k,2}H_{k-2}, & p_{k,3}H_{k-3}, & \cdots, & H_{-1} \end{bmatrix}, \\
 J_{21} &= \begin{bmatrix} p_{k+1,1}H_k \end{bmatrix}, & J_{22} &= \begin{bmatrix} p_{k+1,2}H_{k-1} & p_{k+1,3}H_{k-2} & \cdots & H_0 \end{bmatrix},
 \end{aligned}$$

190 Then, the closed form solution for the first N rows of J^{-1} (the first block) can be written
 191 [4] as

$$[J^{-1}]_{(1:N,:)} \simeq -(J_{22}J_{12}^{-1}J_{11} - J_{21})^{-1} \begin{bmatrix} -J_{22}J_{12}^{-1} & I \end{bmatrix}. \quad (5)$$

192 However, in reality, J is not a finite matrix, but an infinite dimensional matrix. An important
 193 fact to verify, then, is whether there exists a sufficiently large value of k to yield an accurate
 194 inversion. While proving that this inverse converges is outside the scope of this work, we
 195 numerically demonstrate in what follows that after $k = 1$, successive terms do not perceptibly
 196 change the results. Specifically, we solve for $d\mathbf{r}'$ with respect to $d\mathbf{c}$ for $k = 0, 1, 2, 3$.

197 As a reference for translation, at $k = 0$, the approximation becomes

$$d\mathbf{r}' \approx H_0^{-1}K(BP + C)d\mathbf{c},$$

198 and at $k = 1$, we obtain the approximation used in the main text. The 0-th order approxi-
 199 mation at $k = 0$ yields no change (Fig. 1a), where the predicted reservoir states (light gold)
 200 are identical to the original states (dark gold). The first order approximation at $k = 1$
 201 (Fig. 1b) yields a change in the reservoir states that outputs to the expected translation in
 202 spatial coordinates. Taking more terms in the approximation ($k = 2$, Fig 1c; and $k = 3$,
 203 Fig. 1d) yields no perceivable change in either the reservoir states or their outputs.

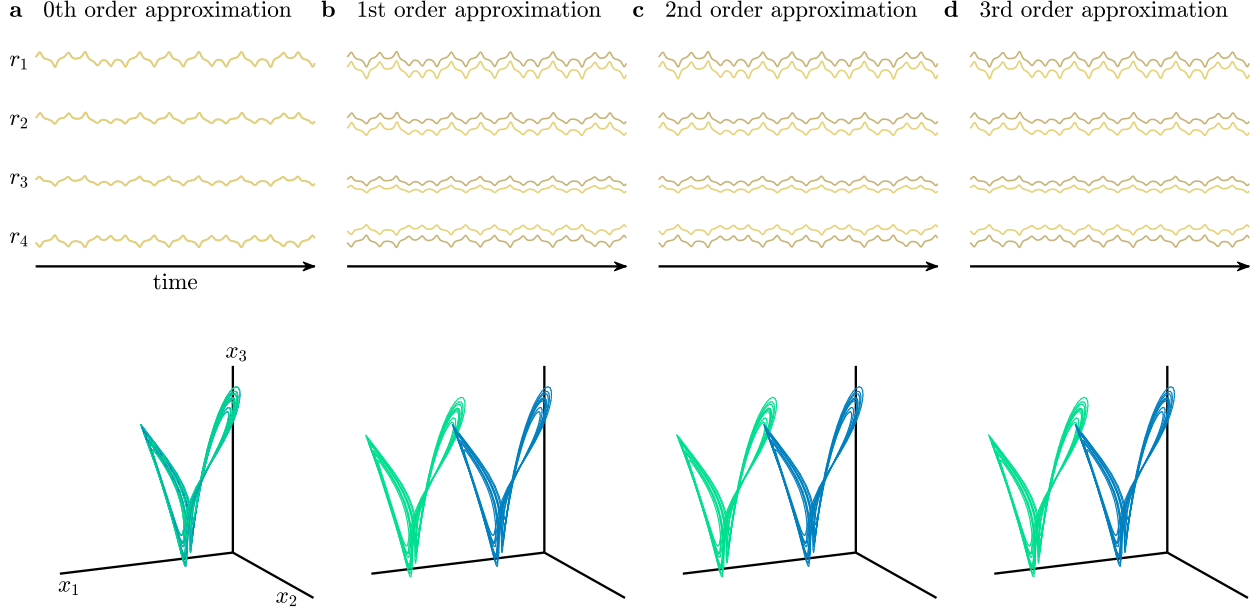


FIG. 1. **Predicted change in reservoir states given a change in control parameter.** Reservoir time series generated by driving the reservoir with the original Lorenz input with $c = 0$ (dark gold), and the predicted time series from solving for dr' after training on translated examples and changing the control parameter $\Delta c = 20$ (light gold), along with their output projections (dark and light red, respectively). These approximations were taken by computing the inverse Eq. 5 for (a) $k = 0$, (b) $k = 1$, (c) $k = 2$, and (d) $k = 3$.

204 H. Summary

205 In sum, we have provided a general form for reservoir dynamics (Eq. 1), the derivation
 206 for the quadratic form of the reservoir (Eq. 2), as well as the dependence of matrices U
 207 and V that arise from the choice of fixed point when using \tanh as the activation function
 208 (Eq. 3,4). We further provide all simulation parameters (time step, Lorenz parameters
 209 and initial conditions, reservoir parameters and initial conditions), along with the specific
 210 details of our simulation method, data dimensions, and training process. Finally, we provide
 211 numerical justification for the truncation of our approximation when deriving the mechanism
 212 of learning (Eq. 5).

213 **II. RESULTS**

214 In this section, we provide some additional results to support the generalizability of the
215 framework.

216 **A. Translation in multiple directions**

217 In the main text, we demonstrated that a reservoir can translate its representation of a
218 Lorenz attractor along the x_1 direction. Specifically, we took an untranslated Lorenz time
219 series $\mathbf{x}_0(t)$, and generated three additional training examples $\mathbf{x}_c(t)$ for $c = 1, 2, 3$ such that

$$\mathbf{x}_c(t) = \mathbf{x}_0(t) + c \begin{bmatrix} 1 \\ 0 \\ 0 \end{bmatrix} .$$

220 We then drove the reservoir using these four training examples and an additional control
221 parameter c that we also varied from $c = 0, \dots, 4$. Afterwards, we performed the feedback,
222 and translated the reservoir's representation by varying the external control parameter c
223 from -40 to 40 . We reproduce this translated representation here (Fig. 2a). We show the
224 same output of the feedback reservoir trained on four examples translated in the x_2 direction
225 ($\mathbf{x}_c(t) = \mathbf{x}_0(t) + c[0; 1; 0]$) and in the x_3 direction ($\mathbf{x}_c(t) = \mathbf{x}_0(t) + c[0; 0; 1]$) (Fig. 2b,c). Hence,
226 we demonstrate that the reservoir can learn these translations in arbitrary directions.

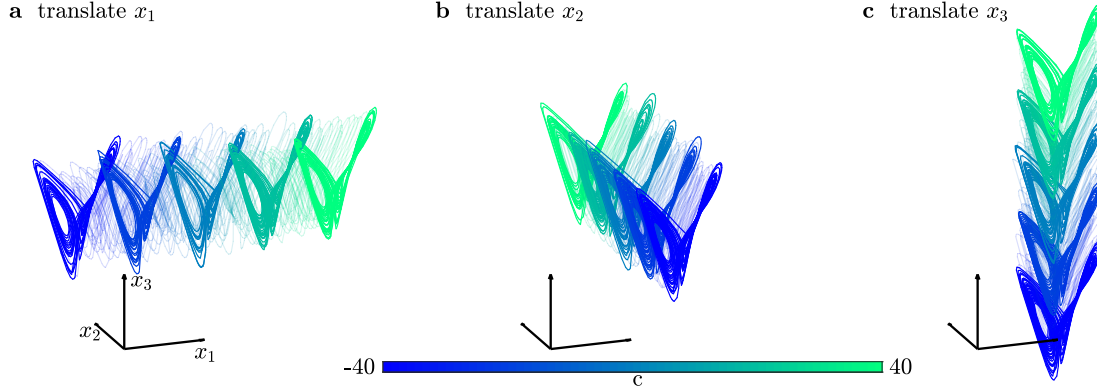


FIG. 2. **Translation of the Lorenz representation in all three spatial directions.** (a) Output of the feedback reservoir after being trained on 4 time series of a Lorenz attractor translated in the x_1 direction at $c = 0, \dots, 4$. By varying c from -40 to 40 , the representation shifts in the x_1 direction. (b) The same scheme is employed for translations in the x_2 direction, and (c) in the x_3 direction.

228 B. Different types of transformations

229 In the main text, we demonstrated that a reservoir trained on the original Lorenz attractor
 230 $\mathbf{x}_0(t)$ and on three transformed examples $\mathbf{x}_c(t) = (I + cP)\mathbf{x}_0(t)$ for $c = 1, 2, 3$, was able to
 231 continuously interpolate and extrapolate the transformation on its internal representation,
 232 even for control inputs between -40 and 40 . Here, we consider a stretch in the x_3 direction,
 233 a shear in the x_1 direction, and a shear in the x_1 and x_2 directions. Specifically, we use the
 234 three matrices

$$P_{\text{stretch},x_3} = \begin{bmatrix} 0 & 0 & 0 \\ 0 & 0 & 0 \\ 0 & 0 & 0.012 \end{bmatrix}, \quad P_{\text{shear},x_1} = \begin{bmatrix} 0 & 0 & 0 \\ 0.012 & 0 & 0 \\ 0 & 0 & 0 \end{bmatrix}, \quad P_{\text{shear},x_1,x_2} = \begin{bmatrix} 0 & -0.012 & 0 \\ 0.012 & 0 & 0 \\ 0 & 0 & 0 \end{bmatrix},$$

235 to train our reservoir for $c = 0, \dots, 4$. For each transformation, we drive the reservoir with
 236 the input Lorenz attractors $\mathbf{x}_c(t)$ and an additional control input c for $c = 0, \dots, 4$. We
 237 then train the reservoir by applying the feedback method used in the main text. Finally, we
 238 drive the autonomous feedback reservoir by varying the control parameter from $c = -40$ to
 239 $c = 40$ for these three transformations (Fig. 3).

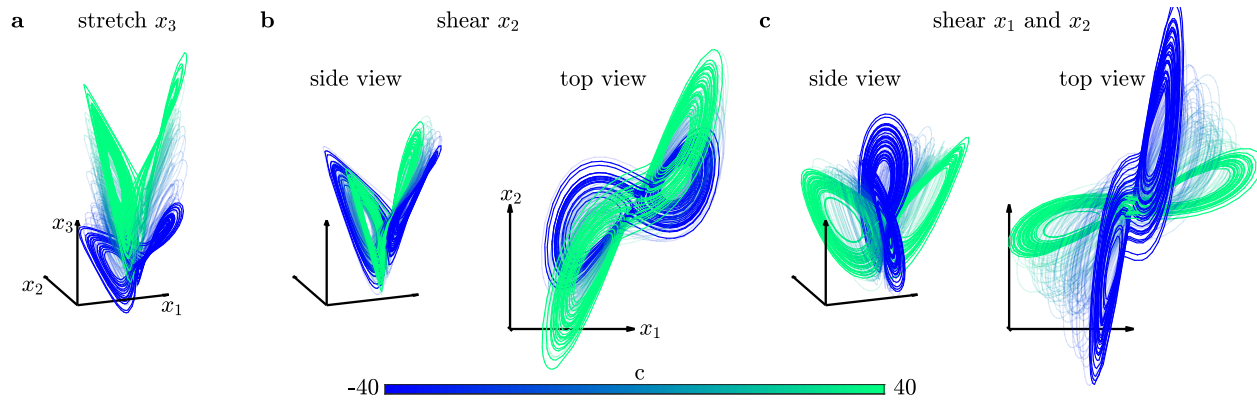


FIG. 3. **Transformation of the Lorenz representation using stretch and shear in several spatial directions.** (a) Output of the feedback reservoir after being trained on 4 time series of a Lorenz attractor stretched in the x_3 direction at $c = 0, \dots, 4$. By varying c from -40 to 40 , the representation stretches in the x_3 direction. (b) The same scheme is employed for a shear in the x_2 direction, and (c) for a shear in the x_1 and x_2 directions.

-
- 241 [1] Lukoševičius, M., Jaeger, H. & Schrauwen, B. Reservoir Computing Trends. *KI - Künstliche*
242 *Intelligenz* **26**, 365–371 (2012).
- 243 [2] Jaeger, H. The “echo state” approach to analysing and training recurrent neural networks –
244 with an Erratum note. *GMD Report* **1**, 1–47 (2010).
- 245 [3] Sussillo, D. & Abbott, L. Generating Coherent Patterns of Activity from Chaotic Neural
246 Networks. *Neuron* **63**, 544–557 (2009).
- 247 [4] Słowik, R. Inverses and Determinants of Toeplitz-Hessenberg Matrices. *Taiwanese Journal of*
248 *Mathematics* **22**, 901–908 (2018).